[1]Jyothi P

[2]G. Pradeepini

Echocardiography Based Cardiac Ischemic Detection Using Red-CNN Classifier

Abstract: - One of the most vital and hardest-working organs of the human body is the Heart. Nevertheless, a condition termed Cardiac Ischemia or CAD is engendered by the inadequate supply of blood along with oxygen to the heart muscle. So, with the aid of a Regularisation Dropout-centered Convolutional Neural Network (ReD-CNN) classifier, an efficient CAD detection system is proposed. At first, the input videos and the data are amassed from the Echonet Dynamic dataset. Next, frame conversion is undergone by the input video. For further processing, keyframes are extracted and preprocessed after frame conversion. Afterward, by means of a Contraction Expansion-Residual Network (CE-ResNet), the heart chambers are segmented, and then the features are extracted. Simultaneously, utilizing the Feynman Kan Formalism-based Tissue Doppler Imaging (FKF-TDI) approach, wall motion is estimated. Meanwhile, the features are extracted from the data and grouped via Average Distance-centric Fuzzy C Means (AD-FCM). After that, mapping of the features extracted from the frames and the grouped features occurs and the resultant data is divided into training, testing, along with validation stages. Then, utilizing the Cosine Similarity-centered Circulatory System Based Optimization (2(CS)BO) methodology, the Feature Selection (FS) is done. Therefore, to compute the Ischemic index, the features that are selected and the estimated wall motions are wielded. Lastly, for effective classification, the Ischemic index and the selected features are fed into the ReD-CNN classifier. Finally, to ascertain the superiority of this technique, the proposed system's performance is contrasted with the prevailing methodologies.

Keywords: Cardiac Artery Disease (CAD), Feynman Kan Formalism-based Tissue Doppler Imaging (FKF-TDI), Average Distance based Fuzzy C Means (AD-FCM), Cosine Similarity-based Circulatory System Based Optimization (2(CS)BO), Regularisation Dropout based Convolutional Neural Network (ReD-CNN).

1. INTRODUCTION

In the lifestyle of the nations, development in the social economy has brought significant changes. Especially, the incidence of cardiovascular risk factors and the number of cases affected by Cardiac Ischemia or Coronary Artery Disease (CAD) increases with the drastic changes in population aging and urbanization (Alizadehsani et al., 2021)[2]. CAD is one of the primary c,auses of death with over 2,200 persons succumbing to it each day as per the statistics from the Centers for Disease Control (CDC) (Ghiasi et al., 2020)[8]. CAD is engendered by the athermanous plaque's accumulation within the walls of coronary arteries. On account of the sudden rupturing of the coronary plaques, plaques occur (W. Li et al., 2022a) [17]. The heart muscle will be impaired owing to ischemic changes if a clot is not treated in time. This engenders ischemia or Myocardial Infarction (MI), or necrosis. Heart attacks or strokes are engendered by CAD and cause higher (i) deaths, (ii) disabilities, as well as (iii) economic loss in industrialized countries than in any other group of diseases (Parisi et al., 2020). For effectual crucial avoidance of MI and death and to lower healthcare costs by evading expensive hospitalizations and interventions, earlier detection and diagnosis of CAD are required (Jalali, Khosravi, et al., 2019)[13].

The death of 50% of men and 64% of women owing to CAD had no former symptoms as per the American Heart Association (AHA) (Jalali, Karimi, et al., 2019)[12]. Yet, a considerable detection gap is engendered by the risk evaluation utilizing conventional risk factors, which encompasses (i) age, (ii) smoking status, (iii) cholesterol levels, as well as(iv) hypertension (De Vita et al., 2019)[5]. For the effective detection of CAD, diverse

[1] [1]Research Scholar, Department of Computer Science and Engineering, Koneru Lakshmaiah Education Foundation, Vaddeswaram Vijayawada, AP, India

Email ID: jyophani.reddy@gmail.com

[2]Professor, Department of Computer Science and Engineering, Koneru Lakshmaiah Education Foundation, Vaddeswaram Vijayawada, AP, India

Email ID: pradeepini_cse@kluniversity.in

Corresponding author Email ID: jyophani.reddy@gmail.com

methodologies are tried and tested clinically. In the prime diagnosis of Heart Diseases (HDs), Electrocardiography (ECG) and Phonocardiogram (PCG) are the two most widely wielded and effective methods. Nevertheless, ECG and PCG are limited in their usage owing to the requirement of very experienced clinical personnel to operate and the non-portability of the equipment (Nishi et al., 2021)[20]. Moreover, for the detection process, coronary angiography is adapted. The angiography technique is not widely accepted owing to severe arrhythmia, allergic reactions, renal toxicity of contrast agents, Vagus reflex, and Invasive Inspection (H. Li et al., 2019)[15]. Thus, blood tests are carried out initially to view the troponin level if a patient has HD symptoms. Doctors can diagnose to some extent centered on the test outcomes whether the patient is suffering as of HD. Long examination time is one of the substantial limitations even though blood tests are wielded to predict the risk of HD(Eskerud et al., 2019)[7]. Therefore, for the diagnosis of Coronary HD (CHD), echocardiography reports are wielded. A non-invasive diagnostic approach to detect the complications of RV infarction, encompassing ventricular septal rupture and severe tricuspid regurgitation is termed Echocardiography. But, the usage of Echocardiography in HDD causes backaches, headaches, and rashes in some patients. These effects are due to the strong firmness given while taking the pictures of the heart. However, Echocardiography is widely utilized in the HDD as it is very effective in detecting heart disease. Some techniques used in the existing works for HDD are Artificial Neural Network (ANN), Support Vector Machine (SVM), K-nearest neighbor (K-NN), Decision tree, AdaBoost (AB), Logistic Regression (LR), Naive Bayes (NB), and fuzzy logic (FL). However, the developed techniques obtained considerably low accurate results due to overfitting problems. As a result, with the aid of a classifier, the ReD-CNN-based HD Detection (HDD) system using Echocardiography is proposed in this paper.

1.1 Problem Definition

There are certain demerits apart from diverse advantages provided by the prevailing CAD detection techniques.

- For the early diagnosis of pre-symptomatic Ischemia HD (IHD), ECG has been recognized as a routine clinical procedure. However, they have lower sensitivity and specificity.

- Huge inconsistencies and variations are exhibited by manual contouring of the epicardial and endocardial walls in echocardiography as it is robustly reliant on the sonographer's training and expertise.

- The majority of the automated classification techniques categorizes wall motion either amid rest or stress and possesses only utilized features extracted as of end-systole along with end diastole frames.

- Since manual processing and expert labeling of ultrasound video frames suffer from both intra- and inter-observer variability, the need for automating cardiac measurements is augmented. Furthermore, it is intricate to efficiently train networks because of the heart's sophisticated anatomical structure.

Therefore, the proposed ReD-CNN-based HDD system is wielded to mitigate the aforesaid issues.

This paper's remaining part is arranged as: The related works concerning the proposed method are reviewed in section 2. Section 3 specifies a brief explanation of the proposed study. Section 4 displays the experimental outcomes. Lastly, section 5 exhibits the conclusion with future work.

2. RELATED WORKS

(Han & Liang, 2021)[10] created a model for the segmentation of the left ventricle in the ultrasonic cardiogram automatically.VGG19-Fully Convolutional Network (VGG19-FCN) and U-Net modelwere wielded for the segmentation. Next, to diagnose patients with CHD, the features were obtained. The efficacy of echocardiographic left ventricular segmentation, which played a vital function in the CHD diagnosis, was ameliorated by the technique. Nevertheless, more time was consumed by the segmentation. So, there was a delay in the prediction outcomes.

(Nilashi et al., 2020)[19] established Fuzzy Support Vector Machine (FSVM) model for CHD diagnosis with self-organizing maps. To lessen the computation time of disease prediction, the incremental Principal Component Analysis (PCA) and FSVM were employed. The accuracy of the HD classification was ameliorated by the usage

of incremental FSVM as per the data analysis on the '2' datasets. Nevertheless, for the overlapped large datasets, the FSVM model couldn't produce accurate outcomes.

(W. Li et al., 2022b) recommended a framework for the prediction of CHD centered on the Combined Reinforcement Multitask Progressive Time-series Network (CRMPTN). Initially, for the pre-training, Deep Reinforcement Learning (DRL) was wielded. After that, the status of CHD was forecasted by diverse modules and progressive time-series networks. The experimental outcomes exhibited that the model outperformed other top-notch methods after DRL pre-training. Nevertheless, inaccurate outcomes would be produced owing to prolonged learning in the model.

(Tama et al., 2020)[23] evinced an intelligent detection system for CHD with an ensemble 2'-Tier Classifier. To choose the most vital feature set on the dataset, a Particle Swarm Optimization (PSO)-centered FS was performed. Regarding accuracy, F1, and Area Under the Curve (AUC), the detection model performed better than the prevailing models. Yet, after certain iterations, the model converged slowly and this deteriorated the model's efficacy.

(Wang et al., 2020)[25] examined a stacking-centered model for the non-invasive detection of CHD. Here, a '2'-level stacking-centered model was modelled in which level 1 was base-level classifiers and level 2 was meta-level. After that, to discover the best-combined classifiers, an enumeration algorithm was wielded. The experimental outcomes revealed that an accuracy of 95.43% was acquired by the model for the detection of CHD. Nevertheless, the model's efficacy was limited since the technique couldn't utilize optimal parameters.

(Chen et al., 2020)[3] put forward a Machine Learning (ML) centered framework for the detection of CAD with coronary bifurcation features. For the coronary bifurcation feature extraction, the morphometric technique was wielded. Then, for the evaluation of the performance utilizing the features, many ML techniques were deployed. With the usage of the grid search optimization methodology, the polynomial Support Vector Machine (SVM) had the best performance for CAD detection as per outcomes. Nevertheless, for training huge datasets, the polynomial-SVM algorithm had speed limitations.

(Joloudari et al., 2020)[14] constructed a system for CAD diagnosis centered on the selection of noteworthy predictive features. So, the ML model's Random Trees (RTs), SVM, and Decision Tree (DT) of Chi-squared Automatic Interaction Detection (CHAID) were examined for the feature's selection. Lastly, the built scheme corroborated that the RTs model surpassed other models. Yet, in RTs, the tree's construction consumed more time to forecast the outputs.

(Shahid & Singh, 2020)[22] established an approach to CAD diagnosis with the PSO-centered Emotional Neural Network (EmNN). For FS, '4' diverse techniques were deployed by the scheme. Furthermore, to ameliorate the network's learning ability, emotional parameters were wielded. The created model's performance was proved by means of the acquired highest average value of (i) accuracy, (ii) precision, along with (iii) f1 score. Nevertheless, in processing big datasets, the datasets wielded were not huge enough for reflecting their usefulness better.

(Abdar et al., 2019)[1] built an ML methodology for the precise diagnosis of CAD. At first, to ameliorate the classifier's efficacy, the data were pre-processed and normalized. Afterward, 10 traditional were wielded in which the parameters were optimized by the New 2level Genetic optimizer (N2Genetic optimizer) and PSO algorithm. An accuracy of 93.08% was offered by the N2Genetic-nuSVM as per the experiment outcomes. Nevertheless, the model was restricted for CAD detection owing to the shortage of data and high time consumption.

(Velusamy & Ramasamy, 2021)[24] constructed a model centered on a heterogeneous classifier's ensemble for the diagnosis along with a forecast of CAD with a lessened feature subset. The ensemble classifier with '3' base classifiers was created. Next, for CAD prediction, the base classifier's outcomes were merged with an ensemble voting technique. The finding investigation exhibited that better classification accuracy was accomplished by the (Weighted-Average Voting Ensemble) WAVEn algorithm. Yet, reliable outcomes weren't produced as the model wielded weak ensemble classifiers.

(Jahmunah et al., 2021)[11] rendered the Gabor Convolutional Neural Network (GaborCNN) model for the automated prediction of (i) CAD, (ii) MI, along with(iii) Congestive Heart Failure (CHF). For the accurate

prediction of normal, CAD, MI, and CHF classes, the Gabor filter was wielded in the CNN. Since the GaborCNN model could be trained faster with lower weights, this model was more efficient than the CNN and it achieved higher accuracy performance. Nevertheless, as a few data for CAD were studied, the overfitting problem could happen.

(Chendeb et al., 2022)[4] launched echocardiography video's semi-supervised segmentation by graph signal processing. GraphECV was the created model. Instance segmentation, construction of a graph utilizing KNN, graph sampling, and finally a semi-supervised learning technique were encompassed in the GraphECV. The investigational results displayed that the GraphECV-centered model outperformed other top-notch methods. Nevertheless, more time was consumed during the node's processing in the GraphECV and the model's speed was lessened.

(Gupta et al., 2022)[9] established a Computer-intelligence system for CAD detection on the Z-AlizadehSani dataset (C-CADZ). For FS, C-CADZ wielded Fixed Analysis of Mixed Data (FAMD) and was trained by means of the RF and Extra Trees (ET) classifiers. Regarding accuracy, the experimentation outcomes exhibited that C-CADZ surpassed the top-notch methods of the last decades. However, when weighed against the C-CADZ model, some of the analogized research provided better outcomes.

(Nasarian et al., 2020)[18] constructed a model to extract the significant features required for CAD detection with a balancing approach. Therefore, Heterogeneous Hybrid FS (2HFS), which was a hybrid FS algorithm, was created. For classification, (i) DT, (ii) Gaussian Naive Bayes (GNB), (iii) RF, and (iv) eXtreme Gradient Boosting (XGBoost) classifiers were wielded. A classification accuracy of 81.23% was yielded by the 2HFS method as per the outcomes. However, the best results couldn't be obtained on the Hungarian and Z-AlizadehSani datasets.

[6] (Dutta et al., 2020)examined an efficient CNN for CHD prediction. Initially, the Least Absolute Shrinkage and Selection Operator (LASSO) centered feature weight appraisal followed by majority-voting centered significant features identification was performed. Next, the significant features were homogenized by the Fully Connected Layer (FCL). When analogized to the individual accuracies of SVM or RF classifiers, the exhibited model's balanced accuracy was better (79.5%). Yet, the output would deviate from the results as weight assessment could lose some data.

3. PROPOSED ECHOCARDIOGRAPHY-BASED HEART DISEASE DETECTION METHODOLOGY

HD is caused by the heart's abnormal functioning due to any reason. The problem of overfitting is present even though various techniques are wielded for the effective detection of HD. So, by employing Echocardiography, an efficient HDD system is proposed. Figure 1 portrays the proposed HDD system's structure.

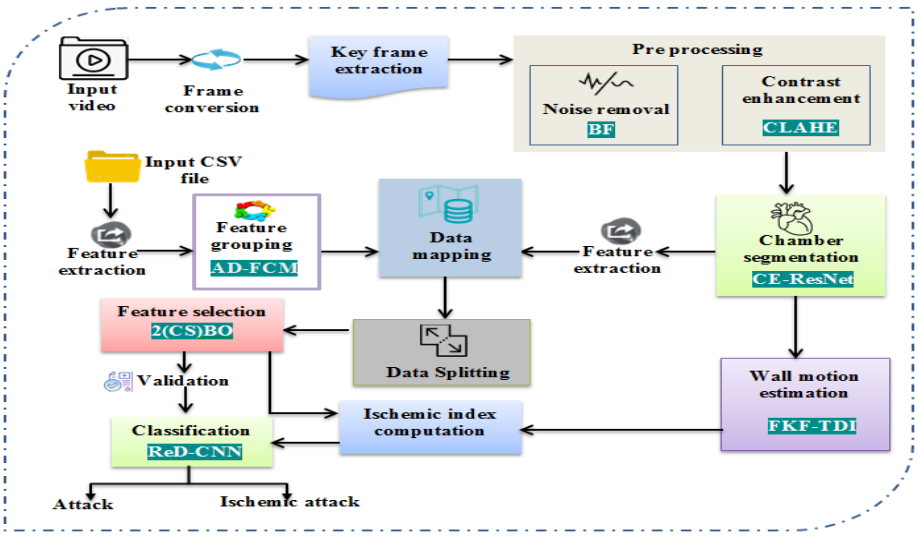

Figure 1: Structure of the proposed methodology.

3.1 Video Processing

Chiefly, the input video that is obtained from the dataset undergoes certain processes and they are explicated below.

3.1.1 Frame Conversion

The input video is obtained from the publically available dataset to start the effective HDD process. Then, utilizing the frame conversion strategy, the acquired input video is converted into multiple frames. Therefore, the frame conversion process is articulated as,

$$F^{v} = \left\{F^{1}, F^{2}, ..., F^{N}\right\} \tag{1}$$

Where, the number of video frames is indicated by N.

3.1.2 Keyframe extraction

After that, from the video frames obtained, keyframes are extracted. In the obtained video frames, more frames are repeated, and the differentiation ratio between the frames is very low. Thus, the computation time of the model was increased due to processing these duplicate frames; so, it is necessary to remove such frames to ameliorate the disease detection efficiency. So, the K- key frames extracted $\left(\hat{F}^{v}\right)$ are delineated as,

$$\hat{F}^{v} = \left\{\hat{F}^{1}, \hat{F}^{2}, ..., \hat{F}^{K}\right\} \tag{2}$$

3.1.3 Pre-processing

To obtain better-processed frames, pre-processing of the extracted keyframes is done. In the proposed work, the '2' pre-processing steps, namely noise removal and contrast enhancement, are entailed. It is elaborated on below.

3.1.3.1 Noise Filter by BF

The most widely wielded filter in image processing that is majorly utilized for smoothing and noise removal is the Bilateral Filter (BF). The BF is a nonlinear, edge-preserving filter used for image pre-processing to smooth the image while edge-preserving. The BF can replace the intensity of each pixel with the weighted average intensity of the nearby pixels based on the Gaussian distribution. Thus, for preserving the sharp edges, the BF utilized the Euclidean distance of pixels and also the radiometric differences like range differences, such as color intensity and depth distance. The BF removed most texture, noise, and fine details, but effectively preserved the large sharp edges without blurring. So, the bilateral filtering process $\left(B(\varphi)\right)$ is denoted as,

$$B(\varphi) = \psi^{-1}(\varphi)\int \eta(\varphi)\hat{F}^{v}(a)\, d(a.\varphi)\, e\left(\hat{F}^{v}(a), \hat{F}^{v}(\varphi)\right) da \tag{3}$$

Here, the bilateral function is ψ^{-1}, the integration variable is symbolized by a, the generic pixel value is denoted by φ, the coordinates in the spatial neighborhood is signified by $\eta(\varphi)$, $\eta(\varphi)$ is specified by d, e, and it is delineated as,

$$d(a, \varphi) = \exp\left(-\frac{\|\varphi - a\|^{2}}{2\mu_{d}^{2}}\right) \tag{4}$$

$$e\left(\hat{F}^{v}(a), \hat{F}^{v}(\varphi)\right) = \exp\left(-\frac{\left(\hat{F}^{v}(\varphi) - \hat{F}^{v}(a)\right)^{2}}{2\mu_{e}^{2}}\right) \tag{5}$$

Here, the standard deviation of the Gaussian function in the spatial domain and range domain is expressed by μ_d and μ_e, which are used to adjust the influence of the weighting function of d, e, respectively. The spatial domain gives the size of the considered neighbourhood, and the range domain denotes the minimum amplitude of an edge. Therefore, N^f symbolizes the noise-removed frame image.

3.1.3.2 Contrast Enhancement using CLAHE

Contrast Limited Adaptive Histogram Equalization (CLAHE) technique is espoused to ameliorate the medical image frame's contrast. The over-amplification of contrast in the video frames is lessened by CLAHE. The CLAHE has three major features, such as tile generation, histogram equalization, and bilinear interpolation. In general, instead of the entire image, it operates on the extracted video frame's minor portion termed tiles. The CLAHE technique uses a clipping limit for the prevention of the over-saturation issue in the high peak region of the image. The high peak region in the histogram of the image tile is due to the same intensities of the frames. The surrounding tiles are blended to remove the false boundaries with the bilinear interpolation. Thus, the CLAHE produced natural-looking images by means of effectively enhancing the contrast of the images by limiting the contrast amplification range to decrease the presence of noise. The CLAHE not only flattens the histogram but also has maximum entropy compared with other histogram equalization techniques. So, the contrast enhancement procedure using CLAHE is elucidated further down,

- First, the incoming frame is divided into numerous continuous and non-overlapping regions to achieve better contrast enhancement by processing each region. Each region is of equal size.

- Further, the obtained regions are grouped into '3' different regions with equally differentiated 64 regions in an image. Here, the Inner Region (IR) of the image contains 36 regions of the image pixels, the Corner Region (CR) consists of only 4 regions, and the Border Region (BR) contains 24 regions. It is devised as,

$$N^f = \left\{N_1^f, N_2^f, N_3^f\right\} \tag{6}$$

Here, the IR, CR, and BR are symbolized by N_1^f, N_2^f, N_3^f.

- Compute the histogram for each region. Next, the clip limit $\left(\varsigma^l\right)$ for the histogram is obtained centered on the limit of contrast expansion (threshold). It is symbolized as,

$$\varsigma^l = \frac{u}{v}\left(1 + \frac{\delta}{100}\left(Q^{\max} - 1\right)\right) \tag{7}$$

Where, the pixels and grayscale values of the region are denoted by u, v, the clip factor is specified by δ, and the maximum clip limit is delineated by $Q^{\max}$.

- After that, the histogram is with a pre-defined threshold. At last, for the resultant contrast-enhanced histograms, the Cumulative Distribution Function (CDF) is obtained. The CDF is defined as the probability of the random variable that is less than or equal to a real number. The CDF is used to describe the behavior of random variables, and the results of CDF are always obtained within 0 and 1. The CDF is a non-decreasing function as the likelihood can either be increased or stay constant depending upon the values. The CDF $\left(\zeta^{(f)}\right)$ is devised as,

$$\zeta^{(f)} = \frac{v - 1}{u} \cdot \sum_{m=0}^{M} H(m) \tag{8}$$

Here, the frame's histogram obtained is indicated by $H(m)$. So, I_p specifies the pre-processed image frame.

3.1.4 Chamber segmentation using CE-ResNet

Subsequently, to obtain the four chambers of the heart, all the pre-processed image frames are segmented. The cardiac ventricle's quantification is essential as it acts as an indicator of certain cardiac ischemic diseases because the chamber's shape varies during the systolic and diastolic cycles. So, in the proposed work, for the heart chamber's effective segmentation, CE-ResNet is applied. Since ResNet overcomes the problem of degradation caused by the rise in network depth, it is wielded for segmentation. In ResNet, the residual block added a shortcut for residual learning to combine the input layer features with the adjacent output layer for solving the degradation problem. Yet, a vanishing gradient problem is undergone by RESNET and the repeated multiplication may make the gradient infinitely small. In the conventional ResNet, the Contraction Expansion (CE) layer is introduced and so, it is termed CE-ResNet. Thus, the CE is a two-stage technique for improving the ResNet system by adding a contraction and expansion path that was utilized in detecting subareas and tiny lesions precisely. The CE-ResNet followed the contracting and expansive path, and the CE procedure was repeated for obtaining the segmented output. The same number of convolution layers added at each block of the encoder structure is applied at each block of the decoder pathway. Both contraction and expansion paths have more sets of weights than U-Net to overcome the vanishing gradient problem. Figure 2 depicts the structure of CE-ResNet. The CE-ResNet-centred segmentation is detailed as follows,

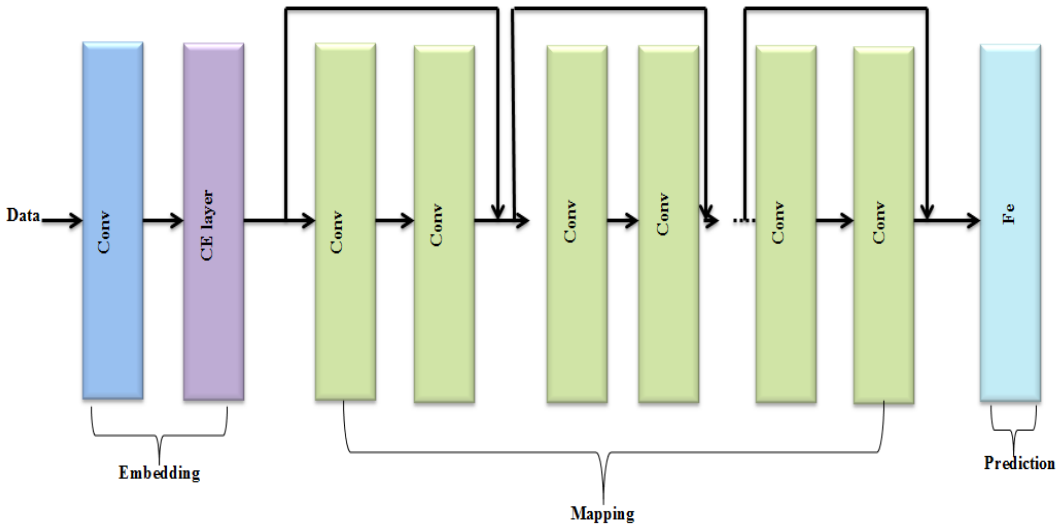

Figure 2: Structure of proposed CE-ResNet

- ***Convolutional layer:*** Chiefly, the preprocessed image frames are fed into the convolutional layer of CE-ResNet. For efficient segmentation of I_p, the stack of convolutional layers with corresponding weight values is introduced in the proposed methodology. So, the stacked convolutional layer output is delineated as,

$$Con(I_p * \varpi) = \sum_{p=1}^{P} (I_p - \gamma^i, I_p - \gamma^j) \cdot \varpi(\gamma^i, \gamma^j) \tag{9}$$

Where, the convolution operation is represented by $*$ and the weight values of i^{th} and j^{th} layers are indicated by $\varpi(\gamma^i, \gamma^j)$.

- ***Contraction and Expansion (CE) layer:*** The convolution layer output is fed into the CE layer. The output of the convolutional layer is obtained as high dimensional features and may be slightly altered, so, to

effectively handle the altered high dimensional features, CE is utilized after the convolutional layer. The heart's proper functioning is affected by a decrease in oxygen as the heart contracts and expands while pumping blood to all parts of the body. So, the subareas and tiny lesions in the heart chambers are accurately detected and segmented in the CE layer. $\overline{Con\left(I_p * \varpi\right)}$ indicates the CE layer output.

- ***Batch Normalization layer:*** Here, The lesion-free output obtained at the CE layer is normalized. Hence, the normalized output $\left(\beta\left(\overline{Con\left(I_p * \varpi\right)}\right)\right)$ is articulated as,

$$\beta\left(\overline{Con\left(I_p * \varpi\right)}\right) = \frac{\overline{Con\left(I_p * \varpi\right)} - M\left(\overline{Con\left(I_p * \varpi\right)}\right)}{\sqrt{V\left(\overline{Con\left(I_p * \varpi\right)}\right)}} \tag{10}$$

Here, the mean value of $\overline{Con\left(I_p * \varpi\right)}$ is referred by $M\left(\overline{Con\left(I_p * \varpi\right)}\right)$, and the variance of $\overline{Con\left(I_p * \varpi\right)}$ is ascertained by $\sqrt{V\left(\overline{Con\left(I_p * \varpi\right)}\right)}$.

- ***Pooling layer:*** A down-sampling operation is performed in this layer. Next, to produce the output with reduced image frame parameters, the normalized output obtained is down-sampled. Then, it is applied to the flattened layer.

- ***Flattened layer:*** In this, the down-sampled image frames are connected to the activation unit of the next layer. Thus, the flattened layer's output is expressed as $\hbar(r)$.

- ***Activation layer:*** ReLU (Rectified Linear Unit) is the activation function wielded in CE-ResNet to present a non-linearity property in the output and it is used in capturing the complex relationship of the data. It is articulated as,

$$\Re\left(\hbar(r)\right) = \max\left(0, \hbar(r)\right) \tag{11}$$

Therefore, the CE-ResNet classifier's output is the segmented chambers and is exemplified as $\wp(Ch)$.

3.1.5 Feature Extraction

For the efficient detection of HD, the segmented chamber features are extracted. Fractal dimension, entropies based on the higher spectra, image texture features, wavelet-based features, local binary patterns, et cetera are some of the handcrafted features extracted as of the segmented chambers. So, mathematically, the set of features extracted $\left(\varepsilon^f\right)$ is articulated as,

$$\varepsilon^f = \varepsilon^1, \varepsilon^2, \varepsilon^3, ..., \varepsilon^F \tag{12}$$

Where, the number of extracted features is exemplified by F.

3.1.6 Wall motion estimation by FKF-TDI

Simultaneously, after the chamber segmentation phenomena, the wall motion abnormality resulting owing to the Ischaemia of the coronary arteries is estimated. For characterizing Ischaemia via the signals generated due to the myocardial motion, Tissue Doppler Imaging (TDI) is the most widely used technique. The TDI is a new echocardiographic technique used for myocardial velocity estimation. The TDI technique is employed for recording the velocity of the systolic myocardial, which is correlated with the ejection fraction. The TDI used ultrasound-based frequency shifts to record the myocardial velocity. Nevertheless, Feynman-Kac Formulism

(FKF) is utilized for its explicity and stableness to compute the velocity of the myocardial contraction based on the diffusion coefficient. It is utilized to overcome the inability of the TDI to distinguish active myocardial contraction due to the adjacent myocardium's tethering effects. The FKF established a link between the parabolic partial differential equations and stochastic processes. Thus, the FKF-TDI reduced the error that occurs in the motion estimation of the frames. Therefore, the proposed technique is termed the FKF-TDI technique. The process is elucidated below,

❖ At first, utilizing spatiotemporal coefficients, the velocity of the wall motion $(\vartheta(\wp(ch), T; H))$ is computed and articulated in (13).

$$\vartheta(\wp(ch), T; H) = \sum_{l,m,n} \Omega\left(\frac{\wp(ch) - \sigma^{l}}{\Delta_{l}}\right)\Omega\left(\frac{\wp(ch) - \sigma^{m}}{\Delta_{m}}\right)\Omega\left(\frac{\wp(ch) - \sigma^{n}}{\Delta_{n}}\right)H^{l,m,n} \tag{13}$$

Where, the grid control points are symbolized by $\sigma = \{\sigma^{l}, \sigma^{m}, \sigma^{n}\}$, the control point spacing at the time T is delineated by $\Delta = \{\Delta_{l}, \Delta_{m}, \Delta_{n}\}$, and the transfer parameter is specified by H, the cubic kernel function transformed the input data into any required form of processing data and it is signified by Ω, the cubic kernel function is used for quantifying the similarity measurements between the pair of data points.

❖ Then, to get a better-estimated value, the obtained velocity is integrated at an interval of (T, τ). In (14), the integrated velocity $(\vartheta^{*}(\wp(ch), T; H))$ is indicated.

$$\vartheta^{*}(\wp(ch), T; H) = \wp(ch) + \int_{0}^{\tau} \vartheta\left(\vartheta^{*}(\wp(ch), T; H), T; H\right)dT \tag{14}$$

By adding $\frac{1}{2}\tilde{\rho}^{2}\Delta z$ in (15), (14) can be discretized via FKF. Therefore, the convection-diffusion expression is unveiled below,

$$\begin{cases} \dfrac{\partial z}{\partial T} + \vartheta^{*}(\wp(ch), w(T))\nabla z + \dfrac{1}{2}\rho^{2}\Delta z & z \in R^{D} \\ z(\wp(ch), 1) = \vartheta(\wp(ch)) & T \in [0,1) \end{cases} \tag{15}$$

Here, the Laplacian operator is Δ, the region of wall estimation is specified by R^{D}, the diffusion coefficient is delineated by $\frac{1}{2}\rho^{2}$, and the network parameter is specified by $W(T)$.

❖ At the time $T = 0$, the above equation becomes,

$$z(\tilde{\wp}(ch), 0) = E[\vartheta(\wp(1)) \mid \wp(0) = \tilde{\wp}(ch)] \tag{16}$$

Where, the expected value of $\wp(1)$ is specified by $z(\tilde{\wp}(ch), 0)$. Hence, the wall motion is efficiently estimated and indicated as $\hat{W}(m)$.

3.2 Data Processing

Further, in the proposed work, for the efficient detection of CAD, the input data obtained from the Comma Separated Values (CSV) file is also processed. The components of the CSV files are the measurements, tracings, calculations, cardiac motion, and chamber sizes. The CSV file data processing is explicated below.

3.2.1 Feature extraction

In the form of a CSV file, the various critical features are extracted in this phase. Filename, Ejection Fraction (EF), which is an evaluation of the amount of blood pumped out by the left ventricle in each contraction, End-Systole Volume (ESV), which is the estimation of blood volume in the ventricle at the systole end, and End-Diastolic Volume (EDV), which is the estimation of blood volume in ventricle before contracts are the features that are extracted from the CSV file data. The extracted features $\left(\xi^{d}\right)$ are characterized below,

$$\xi^{d} = \left\{\xi^{1}.\xi^{2}, \xi^{3}, ..., \xi^{D}\right\} \tag{17}$$

Where, the number of extracted features from the input CSV data is ascertained by D. Next, for feature grouping, these features are fed to the AD-FCM.

3.2.2 Feature Grouping via AD-FCM

The features are grouped together to enhance classification accuracy and detection rate after feature extraction. By utilizing AD-FCM, feature grouping is done in this model. Fuzzy C-Means (FCM) is a clustering technique through which features are assigned to each data. In this, the cluster centers are evaluated randomly. So, the time complexity is increased and detection accuracy is reduced by the initial cluster center's random selection. Optimal cluster centers are identified with AD to conquer this limitation in FCM. This use of AD in Conventional FCM is termed AD-FCM. The following are the AD-FCM steps.

Step 1: At first, the extracted features $\left(\xi^{d}\right)$ are divided into a k number of clusters $\left(Q_{f}\right)$. They are symbolized by,

$$Q_{f} = \left\{Q_{1}, Q_{2}, \cdots\cdots, Q_{k}\right\} \tag{18}$$

Step 2: The membership function $\left(O_{jf}\right)$ is computed and is given by,

$$O_{jf} = \frac{1}{\sum_{f=1}^{F}\left(D_{ij} / D_{if}\right)^{(2/n)-1}} \tag{19}$$

Where, the fuzziness of the membership function is denoted by n and the data points betwixt the clusters and cluster centroids are indicated by D_{ij} / D_{if}.

Step 3:Utilizing equation (20), the cluster centroid c_{p} is estimated.

$$c_{p} = \frac{\sum_{f=1}^{F}\left(M_{jf}\right)^{u} \xi^{d}}{\sum_{f=1}^{F}\left(M_{jf}\right)^{u}} \tag{20}$$

Where, the number of cluster centroids for the k- number of clusters is expressed by $p = 1,2,\cdots M$.

Step 4:By utilizing equation (21), the Euclidean distance $\left(d\left(\xi^d, c_p\right)\right)$ is calculated.

$$d\left(\xi^d, c_p\right) = \sqrt{\sum_{d=1}^{D}\sum_{p=1}^{M}\left(\xi^d - c_p\right)^2} \tag{21}$$

Step 5:Via the threshold value, the objective function $\left(M_{jf}\right)$ is updated by averaging the distance to each cluster. It is given in the expression (22),

$$\widehat{M}_{jf} = \begin{cases} \xi^d to\, c_p & if \sum_{d-1}^{D}\sum_{p=1}^{M}\left(\left\|\xi^d - c_p\right\|\right)^2 < th \\ \min\left(\sum_{d=1}^{D}\sum_{p=1}^{M}\left(\left\|\xi^d - c_p\right\|\right)^2\right) & otherwise \end{cases} \tag{22}$$

Here, the threshold value obtained by averaging the distance betwixt the j^{th} data point and f^{th} cluster is denoted by th.

Step 6: Here, the updated centroid is given as,

$$\widehat{c}_p = \frac{1}{\left|S^d\right|}\sum_{\xi^d \in S^d}\xi^d \tag{23}$$

Where, the total number of data points in the p^{th} cluster is demonstrated by S^d. Therefore, the features are successfully grouped into training, testing, and validation features. It is modeled as,

$$s_g = \left(s_1, s_2, \cdots\cdots, s_G\right) \tag{24}$$

Here, the grouped features are exemplified by s_g and the number of feature groups is indicated by G.

3.3 Data Mapping

Both the features grouped from the data and the features extracted from the image frame are mapped in this phase. Features are mapped accordingly to conform to the geometry at the output location centered on the ID of the video and data ID. Therefore, $m(d)$ represents the mapped data.

3.4 Data splitting

In the data splitting phase, the mapped data is split. Here, the incoming mapped data is split into 75% training, 12.5% testing, along with 12.5% validation. Thus, the output of the data splitting $\left(B_l\right)$ is.

$$B_l = \left\{B_1, B_2, ..., B_L\right\} \tag{25}$$

Where, the $L-$number of splitted data is $l = 1,2,3,...,L$.

3.5 Feature selection using 2(CS)BO

Here, the selection of the most relevant feature from the output of the data splitting is performed. By utilizing 2(CS)BO, FS is carried out. A meta-heuristic optimization algorithm that is inspired by the functioning of the circulatory system is termed CSBO. The CSBO is processed based on the functioning of the body's blood vessels and modeled in two separate groups, namely pulmonary and systemic circuits with two different optimization cycles. The best solution is obtained by analyzing the blood flow into the circulatory system with a new order to circulate through the body. Nevertheless, in the iterative process, the random generation of the blood masses has a lower convergence rate and can easily fall into the local optimum solution in high dimensional space. By utilizing Cosine Similarity (CS), the population generation is done, and by utilizing an S-shaped transfer function, the weaker population is determined to conquer this limitation. By dealing with the feature selection problem, the weakest sorted population enters the pulmonary circulation. Thus, the S-shaped transfer function is applied in all dimensions that define the probability of transforming the position vectors' elements from 0 to 1 and vice versa; thus, the superior fit value is forced to enter the systematic circulation with a novel amount for circulating via the body. The S-shaped transfer function provided a high probability for the blood masses to position switching when the large absolute values of their velocity are far away from the best solution based on the blood flow in the systematic circulation. So, the use of CS in general CSBO is called the 2(CS)BO and it is explicated below.

Step:1Let $B_l = \{B_1, B_2, ..., B_L\}$ (splitted features)be the initial population of blood masses in D dimensional search space. After that, utilizing the CS function $(\cos(\phi))$, the minimum and maximum values of blood masses are generated. Thus, the determination process is articulated as,

$$\cos(\phi) = \frac{\sum_{l=1}^{L} \alpha^{(l)} \gamma^{(l)}}{\sqrt{\sum_{l=1}^{L} \alpha^{(l)}} \sqrt{\sum_{l=1}^{L} \gamma^{(l)}}} \tag{26}$$

Here, the minimum and maximum blood mass values are symbolized by $\alpha^{(l)}$ and $\gamma^{(l)}$.

Step:2By calculating the fitness value $(f(B^l))$ that indicates the possible solution, the movement of blood mass is determined after population initialization. To lessen the classification performance's error rate, it is calculated. It is given in (27).

$$f(B^l) = f(B^1, B^2, B^3, ..., B^L) \tag{27}$$

Step:3 Here, the movement of blood mass in the veins (B_l^{new}) is estimated and is formulated as,

$$B_l^{new} = B_l + \breve{\kappa}_{l1} \times J_l \times (B_l - B^1) + \kappa_{23} \times J_l \times (B^3 - B^2) \tag{28}$$

Where, the direction of motion of l^{th} blood mass is signified by $\breve{\kappa}_{l1}$ and the problem dimension factor is specified by J_l. It is articulated as,

$$\breve{\kappa}_{lm} = \frac{q(B_m) - q(B_l)}{|q(B_m) - q(B_l)| + \zeta} \tag{29}$$

Here, the blood mass dimension is denoted by q and the permittivity constant is ζ.

Step:4 The flow of blood in the pulmonary circulation is determined. In pulmonary circulation, the flow of deoxygenated blood occurs and the blood flow is proportional to the number of weaker populations (w). The blood flow in the pulmonary circulation is modeled as,

$$B_l^{new} = B_l + \left(\frac{RND^N}{ITR} \right) * RND^C(1, D), l = 1 : w \tag{30}$$

Where, the normal random number is RND^N, the iteration number is denoted by ITR, and the randomized Cauchy distribution vector is specified by RND^c. In the meantime, there is also a change in the problem dimension factor. It is delineated as,

$$J_l = rnd(1, D), m = 1 : w \tag{31}$$

Step:5 Later on, the blood flows in the systematic circulation stage. By utilizing the S-shaped transfer function, the number of weaker populations (w) is determined as,

$$w = \frac{1}{1 + e^{-B_l^{new}(T)}} \tag{32}$$

Here, the blood flow in systematic circulation is $B_l^{new}(T)$ and the new position vector $(\Gamma(T))$ is exemplified as,

$$\Gamma(T) = \begin{cases} 1 & RND < S(\Gamma(T+1)) \\ 0 & otherwise \end{cases} \tag{33}$$

Where, the random number is specified by RND, the S-shaped transfer function is delineated by S, and the position vector in the next iteration is indicated by $\Gamma(T+1)$. Next, utilizing (34), the population with better fitness value (R) in the systematic circulation stage $(B_{l,m}^{new})$ is evaluated.

$$B_{l.m}^{new} = B_{1,m} + J_l * (B_{3,m} - B_{2,m}) \tag{34}$$

Here, the dimension vector (J_l) becomes,

$$J_l = \frac{f(B_l) - f_w}{f_b - f_w}, l = 1 : R \tag{35}$$

Where, the best and worst values of the cost function are signified by f_b and f_w. Therefore, until the optimal features are selected, the process is repeated and the number of selected features (y_j) is expressed as,

$$y_j = (y_1, y_2, \cdots\cdots, y_m) \tag{36}$$

Here, the number of selected features is signified by m. For the proposed 2(CS)BO, the pseudocode is elucidated below,

Pseudocode for proposed 2(CS)BO
Input: Splitted features
Output: Selected features
Begin
Initialize the blood mass population $B_l = \{B_1, B_2, ..., B_L\}$

Initialize iteration ITR
For $1 \le l \le L$
Generate $\alpha^{(l)}$ and $\beta^{(l)}$
Determine fitness value $\left(f\left(B^{l}\right)\right)$
Estimate $B_l^{new} = B_l + \tilde{\kappa}_{l1} \times J_l \times \left(B_l - B_1\right) + \kappa_{23} \times J_l \times \left(B_3 - B_2\right)$
Define motion direction $\left(\tilde{\kappa}_{lm}\right)$
For $l = 1: w$

$$B_l^{new} = B_l + \left(\frac{RND^N}{ITR}\right) * RND^C(1, D), l = 1: w$$

Evaluate
Compute dimension factor $\left(J_l\right)$
Evaluate w
Updatenew position vector $\left(\Gamma(T)\right)$
End for
End for
For $l = 1: R$
Calculate $\left(B_{l,m}^{new}\right), \left(J_l\right)$
End for
Return $y_j = \left(y_1, y_2, \cdots\cdots, y_m\right)$
End

3.6 Validation

In this stage, the selected features are validated. Cohen's Kappa Coefficient (CHC) strategy is wielded by the proposed work for validation. The CHC is a statistical model used for detecting the inter-rater reliability and intra-rater reliability of the categorical items. In general, the degree of agreement or disagreement is gauged by how accurately the optimal features are selected or how closely the optimal features are selected, respectively, and D data items are classified into D^* mutually exclusive categories by CHC $\left(E\right)$. In (37), it is modeled.

$$E = \frac{\delta(g) - \delta(h)}{1 - \delta(h)} \tag{37}$$

Here, the total agreement's probability is explicated by $\delta(g)$, and the chance agreement's probability is illustrated by $\delta(h)$. The complete agreement is indicated by $E = 1$.

3.7 Ischemic Index Computation

Here, utilizing a single-valued integrated index called the Ischemic Index, the transparency of the classification process is evaluated. The index value is evaluated by the combination of different features; so, based on these distinct index values, the output classes are also estimated with different ranges. Thus, the transparency of the classification process is estimated based on analyzing distinct index values. The index values are distinctly different for the selected features. The Ischemic Index $\left(I^{i}\right)$is formulated as,

$$I^i = \log_{10}\left(a^f \times \left(d^f + e + d^v\right) - \frac{a^{sm} + n^e + l^{bp1} + l^{bp2}}{b^e} \right) \tag{38}$$

Here, the approximation coefficients are designated by a^f, the fractal dimension is specified by d^f, the entropy function is indicated by e, the detail vertical coefficient is d^v, the angular second moment is signified by a^{sm}, the first and second-order local binary pattern is indicated by l^{bp1}, l^{bp2}, and the normalized and bi-spectral phase entropy is specified by n^e, b^e.

3.8 Classification by ReD-CNN

The selected features (y_j) and Ischemic Index (I^i) are inputted to the ReD-CNN for efficient detection of cardiac Ischemia. The CNN comprises neurons that are self-optimized through training. The CNN architecture has 3 layers, such as the convolutional layer, pooling layer, and fully connected layer. The convolutional layer is the main building block of the CNN and it has a set of filters and parameters, which are learned through training. The pooling layer reduced the size of the feature maps for fast computation. Then, the fully connected layer connects the neurons between the two layers. CNN is employed for solving difficult pattern recognition tasks. Usually, more time is consumed for training and much effort is required to tune the parameters in the Convolutional Neural Network (CNN). The Regularization Dropout (ReD)method is wielded in the two FCLs to overcome this drawback. Thus, HD is classified significantly by the ReD-CNN as a normal and Ischemic attack. The ReD-CNN learns the relevant features from input images and maps them to the corresponding predefined classes, such as normal and Ischemic attacks, enabling accurate image classification. Figure 3 depicts CNN's general structure.

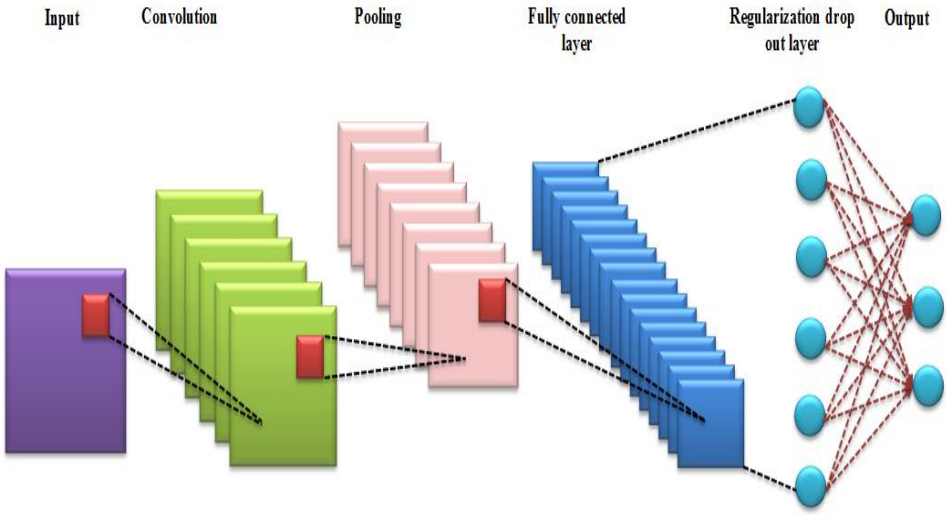

Figure 3: Framework of proposed ReD-CNN

- The selected features (y_j) and Ischemic Index (I^i) are inputted into the classifier. Each layer has its own bias and weight values. The input $(in^{i,j})$ is modeled as,

$$in^{i,j} = \left\{ y_j, I^i \right\} \tag{39}$$

- The input layer's output is forwarded to the convolutional layer. In this, the convolution operation is done and passed to the next layer,

$$C_{cn} = \hbar\left(\sum_{j=1}^{m} \sum_{i=1}^{n} \omega_{cn} * in^{i,j} \right) + \beta_{cn} \tag{40}$$

Here, the weight values of the convolution and input layer are delineated by ω_{cn}, the convolution layer's output is expressed by C_{cn}, and the bias vector is signified by β_{cn}. The activation function is denoted by $\hbar$.

- Next, via a cross-layer aggregation module, the convolution layer's output is processed. The cross-layer aggregation module is utilized here for the extraction of local and temporal features of the output from the convolution layer. After that, by means of the pooling layer, the parameter's spatial size and the dimensionalities of the obtained output are reduced. Thus, the model's computational complexity can be minimized. The relation for the pooling layer (C_{rp}) is given by,

$$C_{rp} = \hbar\left(\sum_{i=1}^{n} \sum_{j=1}^{m} \omega_{rp} * DOWN(C_{cn}) + \beta_{rp} \right) \tag{41}$$

Where, the down-sampling operation is indicated by $DOWN\left(in^{i,j}\right)$. Then, a flattening function is employed to learn the complex patterns of the network to make predictions. Thereafter, to lessen the complexities, the sizes of the data are reduced by the flattening function. The flattening is a pre-processing function, which transforms the high-dimensional output vector from the pooling layer into a one-dimensional vector to decrease the complexity of the process.

- Afterward, to perform the merge operation on the output results of the FCLs and generate data of size n, the Concat() function (regularisation dropout) is wielded. The concatenating operation is defined as the process of concatenating the feature maps from the preceding layers and generating a dense feature map that passes to the further layer. The concatenating function $(C_{po}(g_{ft}))$ is represented by,

$$C_{po}(g_{ft}) = [q_1, q_2, q_3, ..., q_n] \tag{42}$$

- Lastly, utilizing the SoftMaxlayer, the data is classified (D^c). Thus, whether the corresponding cardiac arrest is Ischemic or not is determined by it. Next, by computing the difference betwixt the target value λ_i and the observed values $\widehat{\lambda}_i^*$, the loss function (C_{er}) can be defined as,

$$C_{er} = \sum (\lambda_i - \widehat{\lambda}_i^*)^2 \tag{42}$$

Thereby, the HD is detected accurately and classified as Ischemic or not by the classifier. For the proposed ReD-CNN, the pseudocode is exhibited below:

Pseudocode for proposed CE-ResNet

Input: Selected features, Ischemic index
Output: Classified data
Begin
Initialize weight, bias values
For $1 \le i, j \le m, n$
Input $\left(in^{i,j}\right)$ to convolutional layer
Obtain $$C_{cn} = \hbar\left(\sum_{j=1}^{m}\sum_{i=1}^{n}\omega_{cn} * in^{i,j}\right) + \beta_{cn}$$
Reduce dimension
Compute $$C_{rp} = \hbar\left(\sum_{i=1}^{n}\sum_{j=1}^{m}\omega_{rp} * DOWN\left(in^{i,j}\right) + \beta_{rp}\right)$$
Perform merging
Evaluate $C_{po}(g_{ft}) = [q_1, q_2, q_3, ..., q_n]$
Obtain classified data $\left(D^c\right)$
End for
Calculate loss function $\left(C_{er}\right)$
End

4. RESULTS AND DISCUSSIONS

Here, in comparison with the prevailing schemes, the experimental outcomes of the proposed Ischemic HD classification methodologies are scrutinized. In the working platform of PYTHON, the proposed framework is executed. Figure 4 depicts some of the input images and their corresponding segmented image by the proposed method.

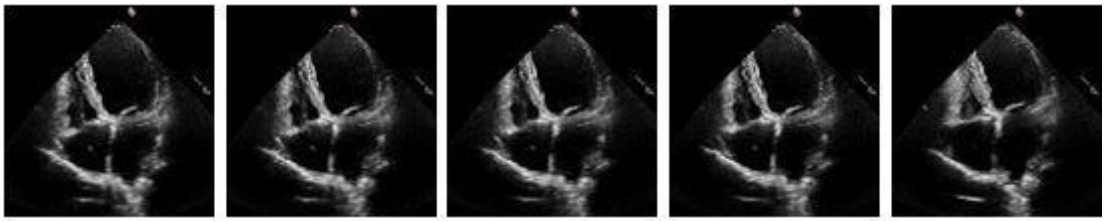

(a)

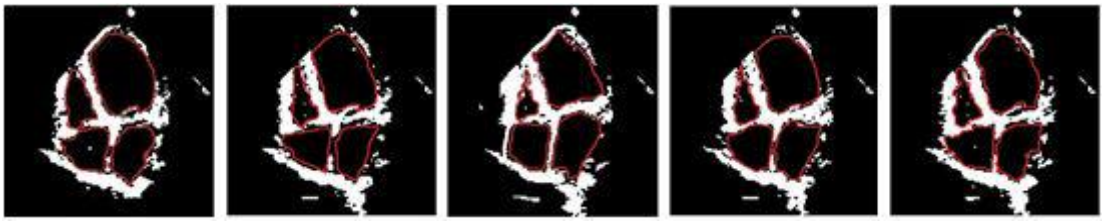

(b)

Figure 4: Sample (a) input images (b) segmented output image on EchoNet-Dynamic dataset

4.1 Dataset description

The experiments are tested on the EchoNet-Dynamic dataset, which is a huge new cardiac motion video data resource meant for medical ML. 10,030 apical-4-chamber echocardiography videos are encompassed in the

dataset. To eliminate the text, every video was cropped as well as masked. After that, the resulting images were down-sampled into standardized 112x112 pixel videos by cubic interpolation.

4.2 Performance Analysis

For three segments namely, segmentation, motion estimation, and classification, the proposed technique's performance is examined.

4.2.1 Performance analysis of the segmentation

Regarding Dice Score (DS), the performance of the proposed CE-ResNet is examined and analogized to the prevailing ResNet, watershed, Otsu, and active contour segmentation algorithms.

Table 1: DS analysis of proposed and existing segmentation algorithms

Algorithms	Dice score
Proposed CE-ResNet	0.9571
ResNet	0.9117
Watershed	0.8667
Otsu	0.8258
Active contour	0.7981

The experimental outcomes of DS analysis of the proposed and the baseline segmentation algorithms are evinced in Table 1. The existing ResNet, Watershed, Otsu, and Active contour models attained the DS values of 0.9117, 0.8667, 0.8258, and 0.7981, respectively. Among the prevailing algorithms, a better DS value (0.9117) is obtained by the ResNet. However, when analogized to the prevailing ResNet, the proposed CE-ResNet obtains 4.97% better DS, that is, 0.9571. This enhancement is owing to the CE's implementation on ResNet. Furthermore, the segmentation efficacy of the CE-ResNet algorithm is proven through this analysis.

4.2.2 Performance analysis of motion estimation

Here, regarding Peak Signal to Noise Ratio (PSNR), the experimental outcomes of the proposed motion estimation algorithm FKF-TDI are comparatively analyzed with the prior TDI, optical flow, block matching, and Pixel Recursive Algorithm (PRA). The PSNR is defined as a ratio between the maximum signal power to the power of distorting noise that affects the quality of the data. The high PSNR values denoted the increased quality of the images.

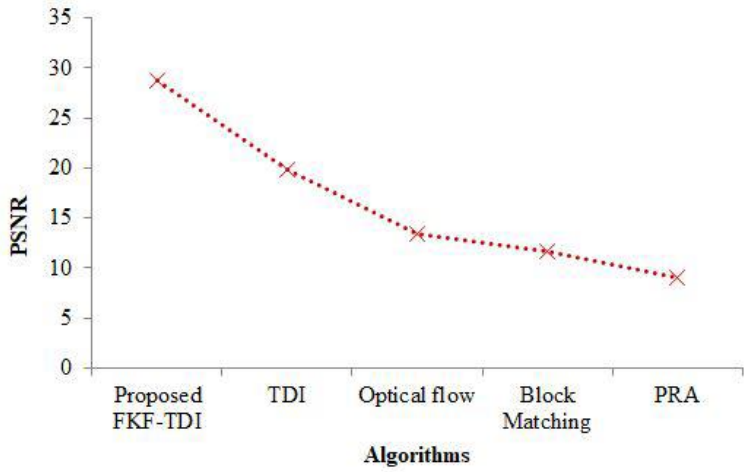

Figure 5: Motion estimation algorithms analysis based on PSNR metric

Since the proposed FKF-TDI has a PSNR value of 28.72dB, it can be proved from Figure 5 that the Image quality of the FKF-TDI is high. Thus, the best PSNR value achieved by the proposed method, as a result of modified FKF-TDI to reduce the errors, occurs within the estimation wall motion of the frames. So, the image quality of

the proposed model is high. A better-quality image is generated by the TDI next to the FKF-TDI algorithm. However, when weighed against all the algorithms, the PRA's image quality is poor due to its stack overflow issue. The best PSNR value for the FKF-TDI algorithm is due to the usage of FKF on the TDI algorithm.

4.2.3 Performance evaluation of classifier

Regarding False Positive Rate (FPR), False Negative Rate (FNR), Negative Predictive Rate (NPR), Matthews Correlation Coefficient (MCC), accuracy, precision, recall, specificity, sensitivity, and computational time, the proposed ReD-CNN classifier's performance is scrutinized in comparison with the prevailing CNN, Artificial Neural Network (ANN), Deep Belief Network (DBN), and Recurrent Neural network (RNN).

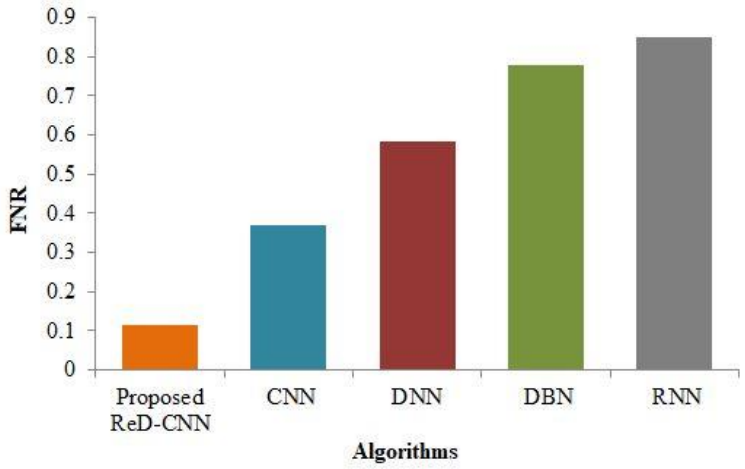

(i)

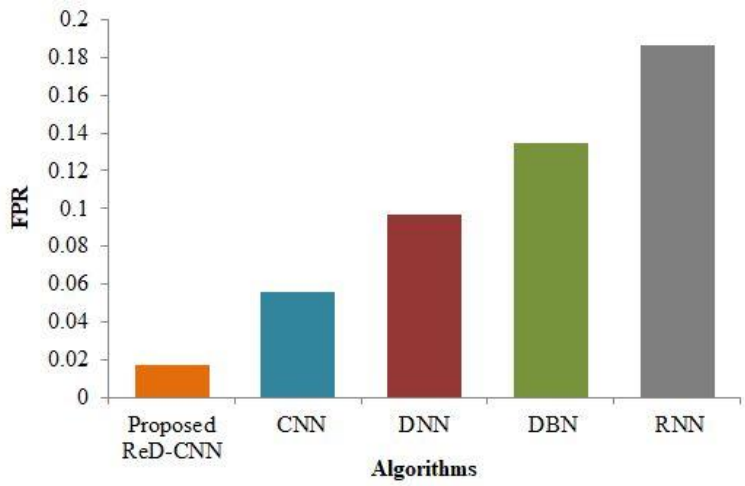

(ii)

Figure 6: Experimental analysis of (i) FNR and (ii) FPR

The experimental results of the (i) FNR and (ii) FPR of the proposed ReD-CNN classifier in comparison with the prevailing baseline classifiers are evinced in Figure 6. When analogized to the prevailing CNN (0.367845), DNN (0.584679), and RNN (0.847965) classifiers, the ReD-CNN classifier has a lower FNR of 0.113467. Furthermore, figure 5(ii) proves that the FPR for the ReD-CNN classifier is lower than the existing algorithm. This is because, the proposedReD-CNN learns the relevant features from input images and maps them to the corresponding predefined classes, such as normal and Ischemic attack; so, it attained minimum error in image classification. Therefore, it is proved that the ReD-CNN model predicts a less number of wrong outputs than the prevailing algorithms.

Table 2: MCC outcomes analysis

Algorithms	MCC
Proposed ReD-CNN	0.92546
CNN	0.74547
DNN	0.53588
DBN	0.44865
RNN	0.26786

The MCC value of the ReD-CNN classifier is evinced in Table 2. The ReD-CNN classifier has an MCC of 0.92546, which is a superior value to the prevailing CNN (0.74547), DNN (0.53588), et cetera. These effective results are obtained by overcoming the overfitting issue in the proposed ReD-CNN. This outcome exhibits that the ReD-CNN model classifies the normal heart data and Ischemic HD data better than the top-notch classifiers.

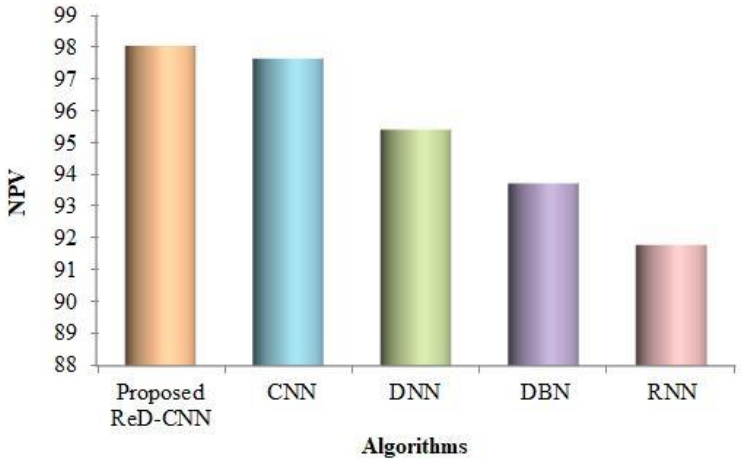

Figure 7: NPV of the proposed model analysis

Figure 7 depicts the Negative Predictive Value (NPV) outcomes of the ReD-CNN algorithm and the prevailing algorithms. The ReD-CNN has the highest (98.04%) NPV followed by the prevailing CNN (97.65%), then DNN (97.42%), etcetera. The ReD is wielded in the prevailing CNN algorithm, which significantly reduces the dimensionality and maximizes the region of the features. So, the better value of the ReD-CNN classifier is achieved.

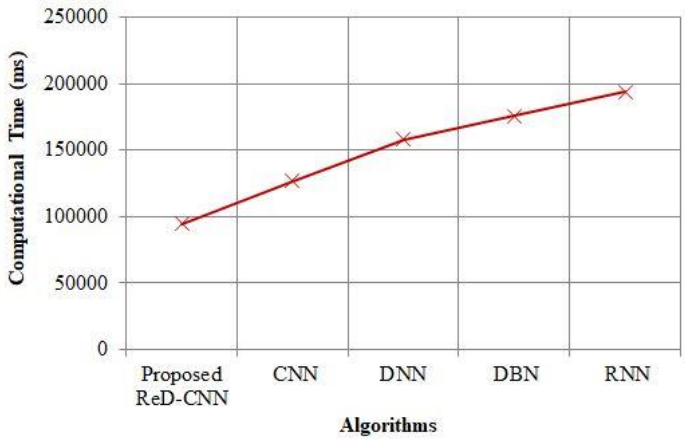

Figure 8: Experimental analysis of computational time

The graphical analysis of the computational time results for the classifier algorithms is portrayed in Figure 8. The ReD-CNN classifier has a computational time of 94328ms, which is 32426ms, 81306ms, and 99460ms less than

the prevailing CNN, DBN, and RNN, respectively. This is obtained as the result of employing ReD in the CNN as it effectively tunes the parameters with minimum time. Hence, it is verified that the ReD-CNN model is more time-effective than all other algorithms.

Table 3: Accuracy, precision, and recall results analysis

Algorithms	**Accuracy (%)**	**Precision (%)**	**Recall (%)**
ProposedReD-CNN	97.94	97.61	96.99
CNN	95.64	95.17	94.67
DNN	93.15	92.86	93.45
DBN	91.73	90.05	91.27
RNN	89.81	88.12	89.44

The accuracy, precision, and recall performance of the ReD-CNN classifier are depicted in Table 3. When analogized to the prevailing CNN, DBN, and RNN algorithms, it is verified from Table 3 that the ReD-CNN classifier generates 2.4%, 6.76%, and 9.05% more accurate results. Moreover, the better performance of the ReD-CNN classifier is proved by the precision and recall results. Thus, it is stated that Ischemic HD could be detected more accurately by the ReD-CNN model than by other techniques.

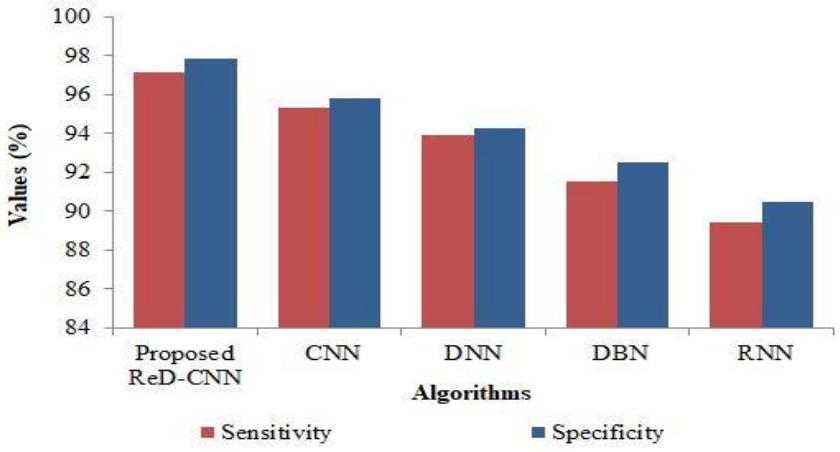

Figure 9: Performance analysis in terms of sensitivity and specificity

It is seen from Figure 9 that the ReD-CNN classifier has a higher specificity of 97.86% than the prevailing CNN (95.79%), DNN (94.29%), and RNN (90.47%). Thus, the higher specificity rate of the proposed ReD-CNN is attained by the effective pattern recognition capability of the proposed model to dynamically classify the normal and Ischemic attacks. This exhibits the ReD-CNN classifier's dominance over other classifiers during HD prediction.

5. CONCLUSION

For the prediction of Ischemic HD, a novel ReD-CNN classifier algorithm is proposed in this paper. CE-ResNet-centered segmentation and FKF-TBI-centered motion estimation are introduced for efficient classification. Next, the proposed ReD-CNN algorithm classifies the input. The proposed system's performance was tested on the EchoNet-Dynamic dataset in which regarding DS, PSNR, accuracy, recall, computation time, NPV, etc., the proposed model's superiority was proved. When analogized to CNN, DNN, and RNN, the proposed ReD-CNN provides 2.56%, 5.11%, and 10.76% more precise results. It is proved by these analyses that the proposed ReD-CNN is more suitable for Ischemic attack detection than the top-notch algorithms. Nevertheless, some discriminant features may not be selected in the proposed model. Therefore, for the identification of more discriminant features, a diverse graph embedding framework will be wielded and the model can be extended to diagnose different stages of ischemic heart attack centered on left ventricle dysfunction in the future.

Declarations

Funding

No funds, grants were received by any of the authors.

Conflict of interest

There is no conflict of interest among the authors.

Data Availability

All data generated or analysed during this study are included in the manuscript.

Code Availability

Not applicable.

Author's contributions

G. Pradeepini and P. Jyothi, contributed to the design and methodology of this study, the assessment of the outcomes and the writing of the manuscript.

REFERENCES

[1] Abdar, M., Książek, W., Acharya, U. R., Tan, R. S., Makarenkov, V., &Pławiak, P. (2019). A new machine learning technique for an accurate diagnosis of coronary artery disease. Computer Methods and Programs in Biomedicine, 179, 1-23. https://doi.org/10.1016/j.cmpb.2019.104992

[2] Alizadehsani, R., Khosravi, A., Roshanzamir, M., Abdar, M., Sarrafzadegan, N., Shafie, D., Khozeimeh, F., Shoeibi, A., Nahavandi, S., Panahiazar, M., Bishara, A., Beygui, R. E., Puri, R., Kapadia, S., Tan, R. S., &Acharya, U. R. (2021). Coronary artery disease detection using artificial intelligence techniques: A survey of trends, geographical differences and diagnostic features 1991–2020. Computers in Biology and Medicine, 128, 1-59. https://doi.org/10.1016/j.compbiomed.2020.104095

[3] Chen, X., Fu, Y., Lin, J., Ji, Y., Fang, Y., & Wu, J. (2020). Coronary artery disease detection by machine learning with coronary bifurcation features. Applied Sciences, 10(21), 1–18. https://doi.org/10.3390/app10217656

[4] Chendeb, M., Darweesh, M., & Al-saad, M. (2022). Semi-Supervised Segmentation of Echocardiography Videos Using Graph Signal Processing. Electronics, 11, 1–14.

[5] De Vita, A., Manfredonia, L., Lamendola, P., Villano, A., Ravenna, S. E., Bisignani, A., Niccoli, G., Lanza, G. A., &Crea, F. (2019).Coronary microvascular dysfunction in patients with acute coronary syndrome and no obstructive coronary artery disease. Clinical Research in Cardiology, 108(12), 1364–1370. https://doi.org/10.1007/s00392-019-01472-4

[6] Dutta, A., Batabyal, T., Basu, M., & Acton, S. T. (2020). An efficient convolutional neural network for coronary heart disease prediction. Expert Systems with Applications, 159, 1-41. https://doi.org/10.1016/j.eswa.2020.113408

[7] Eskerud, I., Gerdts, E., Larsen, T. H., &Lønnebakken, M. T. (2019). Left ventricular hypertrophy contributes to Myocardial Ischemia in Non-obstructive Coronary Artery Disease. International Journal of Cardiology, 286, 1–6. https://doi.org/10.1016/j.ijcard.2019.03.059

[8] Ghiasi, M. M., Zendehboudi, S., &Mohsenipour, A. A. (2020). Decision tree-based diagnosis of coronary artery disease: CART model. Computer Methods and Programs in Biomedicine, 192, 1-43. https://doi.org/10.1016/j.cmpb.2020.105400

[9] Gupta, A., Kumar, R., Arora, H. S., & Raman, B. (2022). C-CADZ: computational intelligence system for coronary artery disease detection using Z-AlizadehSani dataset. Applied Intelligence, 52(3), 2436–2464. https://doi.org/10.1007/s10489-021-02467-3

[10] Han, X., & Liang, G. (2021). Echocardiographic Features of Patients with Coronary Heart Disease and Angina Pectoris under Deep Learning Algorithms. Scientific Programming, 2021, 1-8. https://doi.org/10.1155/2021/8336959

[11] Jahmunah, V., Ng, E. Y. K., San, T. R., &Acharya, U. R. (2021). Automated detection of coronary artery disease, myocardial infarction and congestive heart failure using GaborCNN model with ECG signals. Computers in Biology and Medicine, 134, 1-11. https://doi.org/10.1016/j.compbiomed.2021.104457

[12] Jalali, S. M. J., Karimi, M., Khosravi, A., &Nahavandi, S. (2019). An efficient neuroevolution approach for heart disease detection.Conference Proceedings - IEEE International Conference on Systems, Man and Cybernetics, 2019-October, 3771–3776. https://doi.org/10.1109/SMC.2019.8913997

[13] Jalali, S. M. J., Khosravi, A., Alizadehsani, R., Salaken, S. M., Kebria, P. M., Puri, R., &Nahavandi, S. (2019). Parsimonious evolutionary-based model development for detecting artery disease. Proceedings of the IEEE International Conference on Industrial Technology, 2019-February, 800–805. https://doi.org/10.1109/ICIT.2019.8755107

[14] Joloudari, J. H., Joloudari, E. H., Saadatfar, H., Ghasemigol, M., Razavi, S. M., Mosavi, A., Nabipour, N., Shamshirband, S., &Nadai, L. (2020). Coronary artery disease diagnosis; ranking the significant features using a random trees model. International Journal of Environmental Research and Public Health, 17(3), 1-24. https://doi.org/10.3390/ijerph17030731

[15] Li, H., Wang, X., Liu, C., Wang, Y., Li, P., Tang, H., Yao, L., & Zhang, H. (2019). Dual-input neural network integrating feature extraction and deep learning for coronary artery disease detection using electrocardiogram and phonocardiogram. IEEE Access, 7, 146457–146469. https://doi.org/10.1109/ACCESS.2019.2943197

[16] Li, W., Chen, D., & Le, J. (2020). Coronary Heart Disease Prediction Based on 2020 IEEE International Conference on Bioinformatics and Biomedicine (BIBM)Combined Reinforcement Multitask Progressive Networks. IEEE International Conference on Bioinformatics and Biomedicine, 16 December 2020, 311-318.

[17] Li, W., Zuo, M., Zhao, H., Xu, Q., & Chen, D. (2022b). Prediction of coronary heart disease based on combined reinforcement multitask progressive time-series networks. Methods, 198(2022), 96–106. https://doi.org/10.1016/j.ymeth.2021.12.009

[18] Nasarian, E., Abdar, M., Fahami, M. A., Alizadehsani, R., Hussain, S., Basiri, M. E., Zomorodi-Moghadam, M., Zhou, X., Pławiak, P., Acharya, U. R., Tan, R. S., &Sarrafzadegan, N. (2020). Association between work-related features and coronary artery disease: A heterogeneous hybrid feature selection integrated with balancing approach. Pattern Recognition Letters, 133, 33–40. https://doi.org/10.1016/j.patrec.2020.02.010

[19] Nilashi, M., Ahmadi, H., Manaf, A. A., Rashid, T. A., Samad, S., Shahmoradi, L., Aljojo, N., &Akbari, E. (2020). Coronary Heart Disease Diagnosis Through Self-Organizing Map and Fuzzy Support Vector Machine with Incremental Updates. International Journal of Fuzzy Systems, 22(4), 1376–1388. https://doi.org/10.1007/s40815-020-00828-7

[20] Nishi, T., Yamashita, R., Imura, S., Tateishi, K., Kitahara, H., Kobayashi, Y., Yock, P. G., Fitzgerald, P. J., & Honda, Y. (2021). Deep learning-based intravascular ultrasound segmentation for the assessment of coronary artery disease. International Journal of Cardiology, 333, 55–59. https://doi.org/10.1016/j.ijcard.2021.03.020

[21] Parisi, V., Petraglia, L., Formisano, R., Caruso, A., Grimaldi, M. G., Bruzzese, D., Grieco, F. V., Conte, M., Paolillo, S., Scatteia, A., Dellegrottaglie, S., Iavazzo, A., Campana, P., Pilato, E., Lancellotti, P., Russo, V., Attena, E., Filardi, P. P., &Leosco, D. (2020). Validation of the echocardiographic assessment of epicardial adipose tissue thickness at the Rindfleisch fold for the prediction of coronary artery disease. Nutrition, Metabolism and Cardiovascular Diseases, 30(1), 99–105. https://doi.org/10.1016/j.numecd.2019.08.007

[22] Shahid, A. H., & Singh, M. P. (2020). A Novel Approach for Coronary Artery Disease Diagnosis using Hybrid Particle Swarm Optimization based Emotional Neural Network. Biocybernetics and Biomedical Engineering, 40(4), 1568–1585. https://doi.org/10.1016/j.bbe.2020.09.005

[23] Tama, B. A., Im, S., & Lee, S. (2020). Improving an Intelligent Detection System for Coronary Heart Disease Using a Two-Tier Classifier Ensemble.BioMed Research International, 2020, 1-10. https://doi.org/10.1155/2020/9816142

[24] Velusamy, D., &Ramasamy, K. (2021). Ensemble of heterogeneous classifiers for diagnosis and prediction of coronary artery disease with reduced feature subset. Computer Methods and Programs in Biomedicine, 198, 1-13. https://doi.org/10.1016/j.cmpb.2020.105770

[25] Wang, J., Liu, C., Li, L., Li, W., Yao, L., Li, H., & Zhang, H. (2020). A stacking-based model for non-invasive detection of coronary heart disease. IEEE Access, 8, 37124–37133. https://doi.org/10.1109/ACCESS.2020.2975377